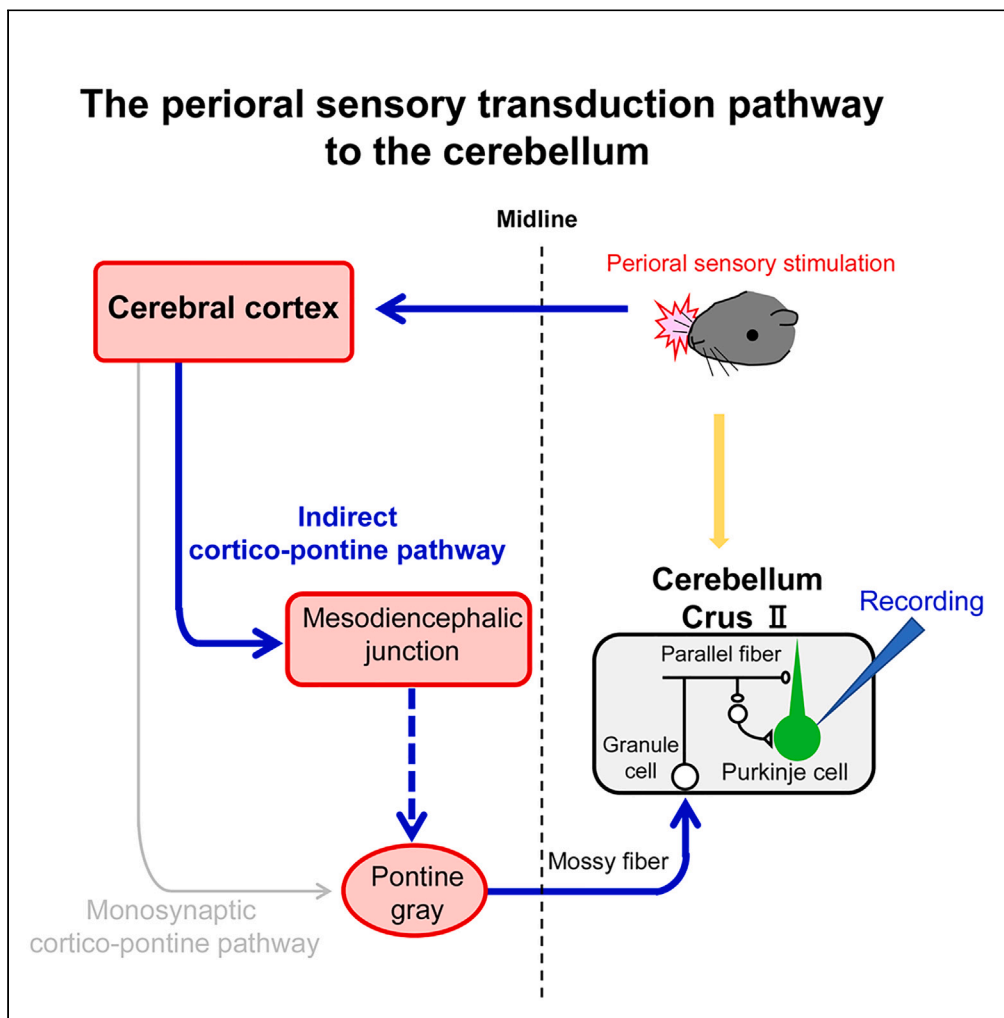


Article

The indirect corticopontine pathway relays perioral sensory signals to the cerebellum via the mesodiencephalic junction



Reika Kubo,
Takayuki Yoshida,
Kenji Yamaoka,
Kouichi
Hashimoto

hashik@hiroshima-u.ac.jp

Highlights

Sensory signals are sent to the cerebellum via the indirect corticopontine tract

The perioral sensory signals are processed in the secondary somatosensory area

Sensory outputs to the pontine nuclei are relayed at the mesodiencephalic junction

Kubo et al., iScience 26, 107301
August 18, 2023 © 2023 The Author(s).
<https://doi.org/10.1016/j.isci.2023.107301>



Article

The indirect corticopontine pathway relays perioral sensory signals to the cerebellum via the mesodiencephalic junction

Reika Kubo,¹ Takayuki Yoshida,¹ Kenji Yamaoka,¹ and Kouichi Hashimoto^{1,2,*}

SUMMARY

In the cerebro–cerebellar loop, outputs from the cerebral cortex are thought to be transmitted via monosynaptic corticopontine gray (PG) pathways and subsequently relayed to the cerebellum. However, it is unclear whether this pathway is used constitutively for cerebro–cerebellar transduction. We examined perioral sensory pathways by unit recording from Purkinje cells in ketamine/xylazine-anesthetized mice. Infraorbital nerve stimulations enhanced simple spikes (SSs) with short and long latencies (first and second peaks), followed by SS inhibition. The second peak and SS inhibition were suppressed by muscimol (a GABA_A agonist) injections into not only the PG but also the mesodiencephalic junction (MDJ). The pathway from the secondary somatosensory area (SII) to the MDJ, but not the cortico–PG pathway, transmitted the second peak signals. SS inhibition was processed in the SII and primary motor area. Thus, the indirect cortico–PG pathway, via the MDJ, is recruited for perioral sensory transduction.

INTRODUCTION

The cerebral cortex and the cerebellum are interconnected (cortico–cerebellar communication loop), and this loop has been proposed to be involved in various cognitive and motor functions.^{1–3} Outputs from the cerebral cortex are thought to be transmitted by the monosynaptic projection to the pontine gray (PG; the basilar pontine nucleus), i.e., the corticopontine projection,^{4–10} and thereafter conveyed to the cerebellum via mossy fibers.^{6,8,11–14} Although the functional roles of the pontine nuclei have been studied,^{15–21} it is largely unknown whether the monosynaptic corticopontine pathway is constitutively recruited for functional signal transduction from the cerebral cortex to the cerebellum.

In rodents, perioral sensory stimulation activates the mossy fiber–granule cell–parallel fiber input pathway through two major signaling streams, and increases simple spike (SS) frequencies at short (4–10 ms) and long (15–22 ms) latencies.^{22–24} These SS enhancements are followed by long SS inhibition.^{23,25–27} Signals for the SS increase with short latency are transmitted by the mossy fiber projections from the brainstem (brainstem–cerebellar pathway), while those with long latency are conveyed by mossy fiber projections from the PG,^{6,8,11–14,28} which are activated by sensory signals from the cerebral cortex.^{1,23,29,30} However, the signaling pathway from the cerebral cortex to the PG involved in perioral sensory transmission is unclear. The prime candidate is the monosynaptic corticopontine pathway; however, little is known about its physiological role in tactile sensory transduction.

We previously reported that perioral sensory signal transduction to the cerebellum via the inferior olive is relayed at the mesodiencephalic junction (MDJ), ranging from around the parafascicular nucleus (PF) to the parvocellular red nucleus,³¹ previously termed the area parafasciculus pruberaris.³² The MDJ receives inputs from the ipsilateral cerebral cortex^{33–36} and sends projections to the pontine gray.^{37–40} These lines of evidence suggest that the MDJ might play a role in sensory signal transmission via pontine nuclei–mossy fiber projections.

In the present study, we aimed to identify the cerebro–cerebellar pathway for perioral tactile signal transduction to cerebellar Purkinje cells (PCs) via the mossy fiber–granule cell–parallel fiber pathway. We found that the perioral sensory signal is transmitted from the cerebral cortex to the PG via the indirect projection relayed at the PF and the rostral part of the midbrain reticular nucleus (MRN) in the MDJ.

¹Department of Neurophysiology, Graduate School of Biomedical and Health Sciences, Hiroshima University, 1-2-3 Kasumi, Minami-ku, Hiroshima 734-8551, Japan

²Lead contact

*Correspondence: hashik@hiroshima-u.ac.jp
<https://doi.org/10.1016/j.isci.2023.107301>



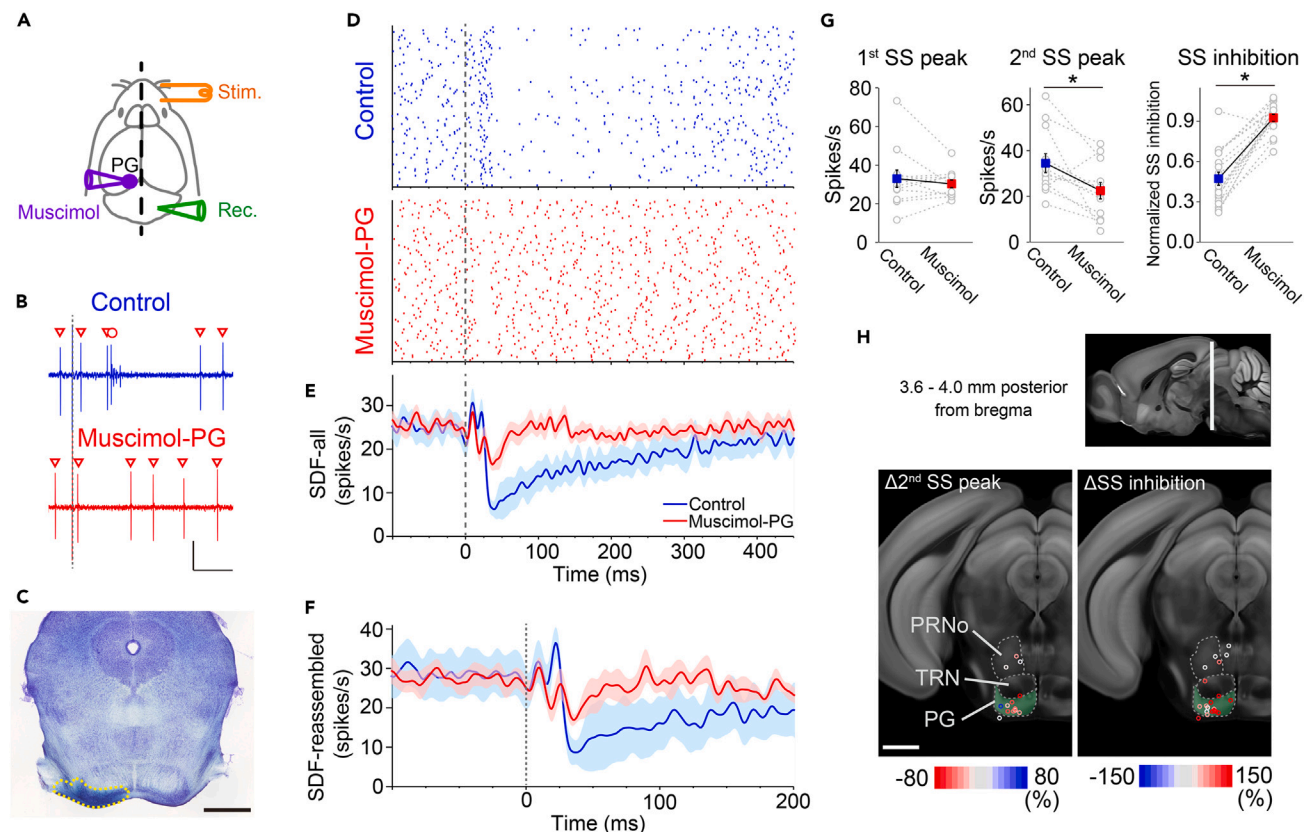


Figure 1. Muscimol injections into the PG suppress the 2nd SS peak and SS inhibition generated by ION stimulation

(A) Schemas of right ION stimulation (orange), recording from a PC in the right cerebellum (green) and the muscimol injection into the left PG (purple). (B) Representative traces of SSs in response to right ION stimulation before (blue) and after (red) muscimol injection into the left PG. SSs and the complex spike are indicated by red triangles and a red circle, respectively. The right ION is stimulated at the dotted line. (C) The muscimol injection site identified by co-injected Chicago Sky Blue into the left PG (yellow dotted line). (D) Representative raster plots of SSs from 100 trials of ION stimulation before (blue) and after (red) muscimol injection into the left PG. Dotted lines represent ION stimulus onsets. (E and F) Peri-stimulus spike density function (SDF) of SSs in response to ION stimulation before (blue) and after (red) muscimol injection into the left PG. Data are for all PCs (E; $n = 12$, from 12 mice) and reassembled data with clear 1st and 2nd SS peaks (see STAR Methods) (F; $n = 9$, from 9 mice). Lines and shaded areas indicate mean and SEM, respectively. (G) Changes in 1st SS peak (left), 2nd SS peak (middle) and normalized SS inhibition (right) caused by muscimol injection into the PG. The 1st and 2nd SS peaks are summarized from reassembled data with clear peaks (F), and normalized SS inhibition is summarized from all data (E). Averaged data for control (blue) and muscimol-injected (red) mice are presented as mean \pm SEM. Muscimol injections into the PG significantly suppressed the 2nd SS peak and SS inhibition, but not the 1st SS peak (paired t -test or Wilcoxon signed-rank test, $*p < 0.05$). (H) Summary of centers of muscimol injection sites in the coronal plane. Injection sites were aligned to the Allen Mouse Common Coordinate Framework (CCFv3).^{41,42–44} (upper) The position of lower panel images is indicated by the white line. (lower) Pseudocolor codes for Δ 2nd SS peaks (left) and Δ SS inhibition (right) were calculated as described in STAR Methods. It should be noted that the color code is inverted between the Δ 2nd SS peak and Δ SS inhibition. Scale bars: 1 mV, 50 ms (B) and 1 mm (C, H). See also Figures S1, S3–S6, and Table S1.

RESULT

The 2nd SS peak and SS inhibition are transmitted via the PG

We recorded SSs evoked by right infraorbital nerve (ION) stimulation from PCs in the right Crus II in ketamine/xylazine-anesthetized mice (Figure 1A).³¹ The electrical stimulation can activate multiple axons at the same time and evoke SSs at a more fixed latency than mechanical perioral tactile stimulation. This allows analysis of multiple temporal events in detail.²⁷ As reported previously,^{22–24} the SS firing rate was enhanced around 5–15 ms (1st SS peak) and 20–33 ms (2nd SS peak) after right ION stimulation (Figures 1B and 1D–1F). Thereafter, SS firing was strongly suppressed at around 40–200 ms after stimulation (SS inhibition) (Figures 1B and 1D–1F).^{23,25–27} The SS inhibition was elicited by relatively weak intensity (0.2 mA) ION

stimulation (Figure S1). SS inhibition gradually increased with increasing stimulus intensity, but tended to plateau at large stimulus intensities.

To clarify the sensory signal transduction pathway, we locally applied a GABA_A receptor agonist, muscimol, and analyzed its impact on SS generation.³¹ We first examined involvement of the PG, a major hub of the cerebro-cerebellar pathway, in perioral sensory transduction (Figure 1). The 2nd SS peak was consistently suppressed by local injection of muscimol targeting the left PG (Figure 1C), but the 1st SS peak was not (Figures 1B, 1D, and 1E). The 1st and 2nd SS peaks were sometimes not clearly observed in some PCs. Therefore, we reassembled data with clear first and second peaks larger than the baseline SS firing (see STAR Methods) (Figure 1F, Table S1). The results confirmed that only the second peak was clearly suppressed by muscimol injection into the PG (Figures 1F–1H). In addition, the SS inhibition was shortened by muscimol injection into the PG (Figures 1D–1H), suggesting that the SS inhibition was also mediated by signal transduction via the PG. These results confirmed that sensory signals for the 2nd SS peak and SS inhibition are relayed by the PG.

The 2nd SS peak and SS inhibition are suppressed by muscimol injection into the MDJ

Our previous report showed that the tactile sensory signal to the contralateral inferior olive is relayed by the contralateral MDJ.³¹ We therefore examined the functional roles of the brain areas, ranging from the midbrain to the pons, in sensory transduction using local injections of muscimol (Figure 2). We locally injected muscimol into the left MDJ contralateral to the ION stimulation, and found that the 2nd SS peak and SS inhibition were significantly suppressed (Figures 2A–2D). Effective injection sites were largely localized to the PF and the rostral part of the MRN, anterior to the rostral border of the red nucleus (2.9 mm posterior to the bregma) (Figures 3A–3C and 3H, Table S1). Suppression levels of the 2nd SS peak and SS inhibition varied between PCs, but there was a weak, but significant correlation between them (Figure 3D). Muscimol injections into the right MRN were less effective (Figures 3A–3C). The injections into the PF or the rostral MRN did not significantly affect the 1st SS peak (Figures 2A–2D). Because the area around the PF and MRN in the MDJ is not a source of mossy fibers,^{45,46} it likely relays sensory signals to precerebellar nuclei emerging mossy fibers. To test whether the MDJ and the PG were in parallel or in series in the signal transduction pathway, we injected muscimol into the MDJ and the PG simultaneously, and compared its effect with that of injection into the PG or MDJ only (Figures 2M–2Q). If these pathways function in parallel, the blocking of both of these pathways should result in further suppression. However, simultaneous muscimol injection into the MDJ and the PG did not cause additional suppression of the 2nd SS peak or SS inhibition (Figures 2N–2Q), which suggests that the MDJ and the PG are involved in series in the same signaling stream. These data collectively suggest that the MDJ relay the sensory signals to the PG. In the following experiments, the PF and the rostral MRN are collectively referred to as the MDJ.

We unexpectedly found that muscimol injections into the area ranging from the caudal part of the left pontine reticular nucleus caudal part (PRNc) to the rostral part of the left gigantocellular reticular nucleus (GRN) also effectively suppressed the 2nd SS peak and SS inhibition (Figures 2I–2L, 3A–3C, and 3E–3H). Muscimol injections into the magnocellular red nucleus (RN) and regions dorsal to the PG, such as the pontine reticular nucleus oral part (PRNo) and the parabrachial nucleus (PB), which are interposed among the MDJ, PG and PRNc, were largely ineffective (Figures 2E–2H, 3A–3C, and 3E–3H). In all injections, the 1st SS peak was unaffected (Figures 2D, 2H, and 2L). To identify effective injection site clusters, we classified injection sites by hierarchical clustering using 3D coordinates of the brain and Δ SS inhibition of individual injection sites (Figure 3E). Evaluation of Δ SS inhibition was more reliable and robust to noise than evaluation of the 2nd SS peak because the normalized SS inhibition was calculated using the average SDF at 40–200 ms, but the 2nd SS peak was assessed by a peak SS SDF at a single time point (STAR Methods). We identified nine clusters, including three injection sites that strongly suppressed SS inhibition (clusters 4, 6 and 7; Figures 3E–3H) and others that were less effective (clusters 1, 2, 3, 5, 8 and 9). The effective clusters were concentrated in the PG (cluster 6), MDJ (cluster 4) and PRNc (cluster 7). The presence of isolated effective clusters suggests that the suppression by muscimol was not caused by broad muscimol diffusion to the PG (discussed later).

Although electrical stimulation of the ION is suitable for aligning response latencies, it is an artificial approach. We therefore tested whether muscimol injections into the MRN also suppressed SS generation produced by a more natural type of stimulation, air puffs. SSs were elicited by air puffs to the perioral region (Figure 4A). Muscimol injections into the left rostral MRN (Figure 4E) similarly suppressed the 2nd SS peak

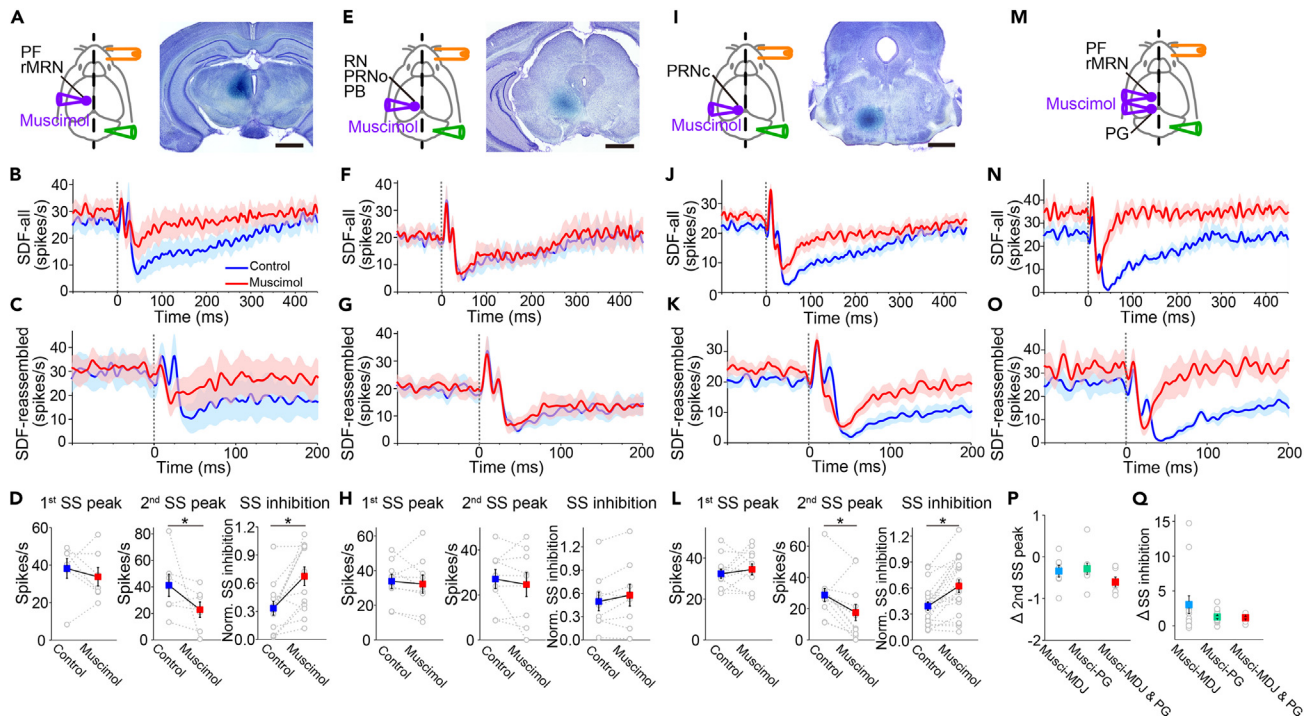


Figure 2. Muscimol injection into the MDJ or PRNc suppresses the 2nd SS peak and SS inhibition generated by ION stimulation

(A, E, I) (Left) Schemas for ION stimulation (orange), PC recording (green) and muscimol injection (purple) into the left MDJ (A, PF and rostral MRN (rMRN)), RN, PRNo and parabrachial nucleus (PB) (E), or PRNc (I). (Right) Muscimol injection sites.

(B, F, J) Peri-stimulus SDFs of SSs in response to right ION stimulation before (blue) and after (red) muscimol injection into the left MDJ (B), RN, PRNo and PB (F), or PRNc (J). Data for all recorded PCs are presented (MDJ (B; n = 13, from 13 mice), RN, PRNo and PB (F; n = 9, from 9 mice), and PRNc (J; n = 21, from 21 mice)). Lines and shaded areas indicate mean and SEM, respectively.

(C, G, K) Similar to B, F, J, but data for PCs with clear 1st and 2nd SS peaks are presented (MDJ (C; n = 7, from 7 mice), RN, PRNo and PB (G; n = 9, from 9 mice), and PRNc (K; n = 12, from 12 mice)).

(D, H, L) Changes in 1st SS peak (left), 2nd SS peak (middle) and normalized SS inhibition (right) by muscimol injections into the MDJ (D), RN, PRNo and PB (H), or PRNc (L). Paired t-test or Wilcoxon signed-rank test, *p < 0.05. Averaged data for control (blue) and muscimol-injected (red) mice are presented as mean ± SEM.

(M) Schemas for ION stimulation (orange), PC recording (green) and muscimol injection (purple) into the left MDJ and PG.

(N) Peri-stimulus SDFs of SSs in response to right ION stimulation before (blue) and after (red) muscimol injection into the left MDJ and PG. Data for all recorded PCs are presented (n = 9, from 9 mice).

(O) Data for PCs with clear 1st and 2nd SS peaks are presented (n = 6, from 6 mice).

(P and Q) Changes in Δ 2nd SS peak (P, MDJ; n = 7, PG; n = 9, MDJ & PG; n = 6, p = 0.2708, one-way ANOVA) and Δ SS inhibition (Q, MDJ; n = 13, PG; n = 18, MDJ & PG; n = 9, p = 0.1503) by muscimol injections. Scale bars: 1 mm (A, E, I). See also Figures S1, S3–S7, and Table S1.

and SS inhibition (Figures 4B–4E, Table S1), suggesting that the pathway for SSs evoked by ION stimulation is identical to that for tactile perioral sensory transduction.

The MDJ and PG receive strong innervations from the secondary somatosensory cortex and the primary and secondary motor cortices

We next investigated the functional connections from the cerebral cortex that are crucial for perioral sensory signal transduction to the cerebellum.²³ We mainly focused on the pathway involving the MDJ in the following experiments because previous reports show that it receives strong ipsilaterally predominant cortical projections.^{33–36} Initially, we examined the distribution of cortico–MDJ and cortico–PG neurons in the cerebral cortex (Figures 5A–5H). Cortico–MDJ and cortico–PG neurons in the left cortex were visualized by injection of retrogradely transported AAV vectors expressing the GFP and ArchT fusion protein into the left MDJ or PG (Figures 5A, 5B, 5E, and 5F). GFP-positive cortico–MDJ neurons were pyramidal neurons in the layer V and were widely distributed in the primary (MI) and secondary (MII) motor cortices,^{33,34,47} but were rare in the primary somatosensory cortex (SI) (Figures 5C and 5D). In addition, a cluster of retrogradely labeled pyramidal neurons was found in the secondary somatosensory area

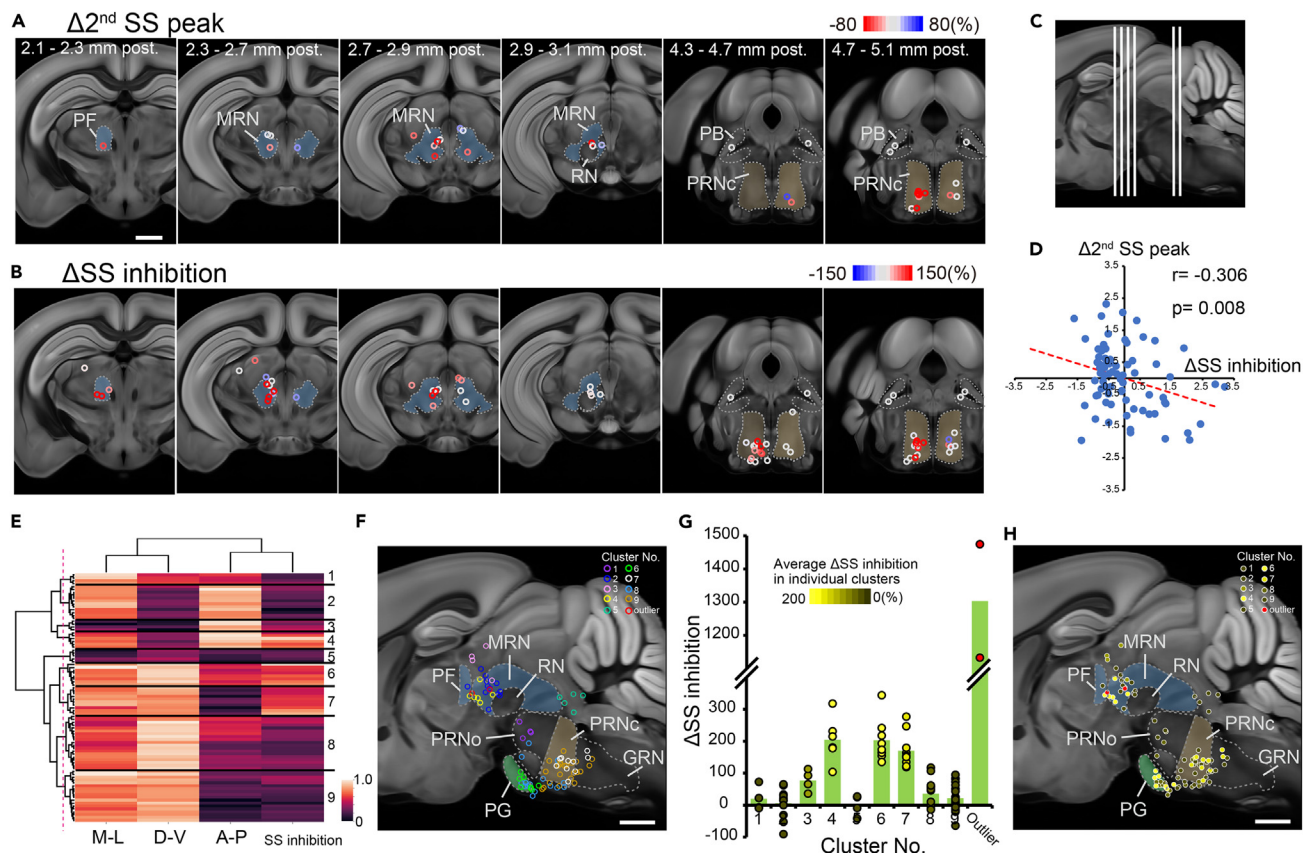


Figure 3. Distribution of muscimol injection sites in the MDJ, pons and medulla

(A and B) Effects on the 2nd SS peak (A; $n = 46$, from 46 mice) and SS inhibition (B; $n = 78$, from 78 mice) at individual muscimol injection sites in the coronal plane at 2.1–2.3 mm, 2.3–2.7 mm, 2.7–2.9 mm, 2.9–3.1 mm, 4.3–4.7 mm and 4.7–5.1 mm caudal to the bregma (left to right panels). Injection sites were aligned to the Allen Mouse Common Coordinate Framework (CCFv3). Pseudocolor coding is as in Figure 1H.

(C) Sites of images in A and B are sequentially shown rostrocaudally.

(D) Relationship of standardized data between Δ SS inhibitions and Δ 2nd SS peaks. Correlation coefficient was calculated from PCs with both 2nd SS peak and SS inhibition data in Table S1 ($n = 76$). No. 3 in Table S1 was omitted from this analysis because it was an outlier. $R = -0.306$, $p = 0.008$; Spearman's rank order test.

(E) Dendrogram and heatmap of hierarchical clustering. The 3D coordinates (antero-posterior, dorso-ventral and medio-lateral) of the Allen Mouse Common Coordinate Framework (CCFv3) and Δ SS inhibition of individual injection sites were used as data for hierarchical clustering. Nine identified cluster numbers are presented on the right side of the graph. All data of the ION stimulation in Table S1, except injections into the right-side brain, were used. No. 3 and No. 6 injection sites in Table S1 are omitted from this analysis because they were outliers (red circles in F and H).

(F) Summary of centers of muscimol injection sites color coded by cluster# shown in E in the sagittal plane ($n = 89$, from 89 mice).

(G) Average (green bars) and individual data (circles) of Δ SS inhibition in 9 clusters. Individual data are color-coded (inset) according to average Δ SS inhibition in each cluster (values indicated by green bars). Two outliers (red circles) are presented on the right side.

(H) Distributions of effective (4, 6 and 7) and ineffective (1, 2, 3, 5, 8 and 9) clusters. The color-coding is as in G. Three distinct effective clusters are in the MDJ (cluster 4), PG (cluster 6) and PRNc (cluster 7). Scale bars: 1 mm (A, F, H). See also Figures S3–S7, and Table S1.

(supplemental somatosensory area, SII). GFP-positive cortico–PG neurons were also layer V pyramidal neurons and were distributed widely in the cortex, from the SII to the MII, as reported previously^{4–10} (Figures 5G and 5H). These results suggest that both the MDJ and PG receive strong inputs from the MI, MII and SII.

Signals for the 2nd SS peak are transmitted via the SII–MDJ pathway

We next examined the functional roles of the cortico–MDJ and cortico–PG pathways in perial sensory transduction. The cortico–MDJ and cortico–PG neurons expressing ArchT–GFP were optically suppressed by systematic light illumination during ION stimulation. Unexpectedly, the SS inhibition was shortened, even in control experiments, after the removal of the left skull (Figure S2), probably because of broad exposure of the cerebral cortex for systematic light illumination, from the MII (medial) to the SII (lateral).

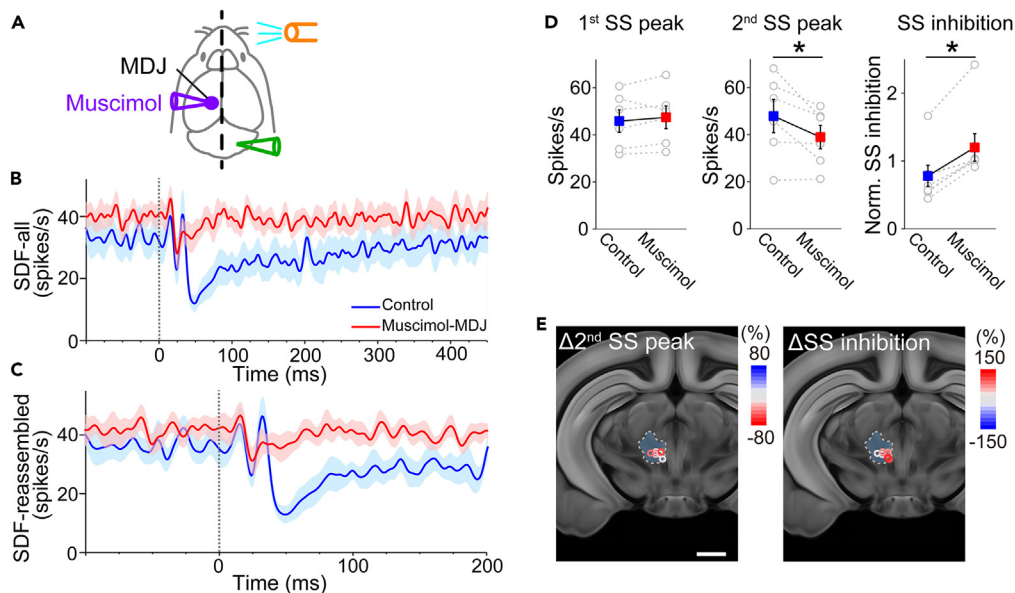


Figure 4. Muscimol injection into the MDJ suppresses the 2nd SS peak and SS inhibition evoked by air puff stimulation

(A) Schema for air puff stimulation (orange), muscimol injection (purple) and recording (green) sites. (B and C) Peri-stimulus SDFs of SSs evoked by right perioral stimulation (20 ms, 0.34 MPa) before (blue) and after (red) the muscimol injection. Data from all PCs (B; $n = 7$, from 7 mice) and PCs with clear 1st and 2nd SS peaks (C; $n = 6$, from 6 mice) are presented. Lines and shaded areas indicate mean and SEM, respectively. (D) Changes in the 1st SS peak (left), 2nd SS peak (middle) and SS inhibition (right) caused by muscimol injection into the MDJ. The 1st and 2nd SS peaks are summarized from reassembled data with clear peaks (C), and SS inhibition is summarized from all data (B). Averaged data for control (blue) and muscimol-injected (red) cells are presented as mean \pm SEM. Muscimol injections into the MDJ significantly suppressed the 2nd SS peak and SS inhibition, but not the 1st SS peak (paired t -test, $*p < 0.05$). (E) Summary of centers of muscimol injection sites in the coronal plane. Injection sites were aligned to the Allen Mouse Common Coordinate Framework (CCFv3). Scale bar: 1 mm. See also Figure S6 and Table S1.

Therefore, we assessed only the 2nd SS peak in the following optogenetic experiments. Light illumination was systematically delivered with an optical fiber of 400 μm diameter to the left mediolateral cortical area that covered the MI/MII and the SII, corresponding to the area with clusters of retrogradely-labeled neurons (Figures 5I, 5J, and 5N). In the case of AAV injection into the MDJ, optical inactivation of the most lateral part of the cortex, roughly corresponding to the SII according to the Allen Mouse Common Coordinate Framework (CCFv3),^{41,42–44} significantly suppressed the 2nd SS peak (Figures 5K and 5L), but that of the medial part around the MI/MII did not (Figures 5K and 5M). In comparison, optical inactivation of the cortico–PG pathway (Figure 5N) did not suppress the 2nd SS peak (Figures 5O–5Q), except for the MI–PG pathway, in which the 2nd SS peak was instead slightly enhanced (Figures 5O and 5Q). These findings suggest that the perioral sensory signal for the 2nd SS peak is transmitted by the SII–MDJ pathway, but not by cortico–PG pathways.

Signals for SS inhibition are relayed at the SII and MI

Although the corticofugal pathways involved in SS inhibition were unclear because of experimental limitations (Figure S2), we examined the role of the cerebral cortex in SS inhibition using muscimol injections through a small craniotomy hole, in which SS inhibition was preserved. Muscimol injection into the left SII and the lateral edge of the SI clearly suppressed the 2nd SS peak (Figures 6A–6E and 6K), confirming the results of the optogenetic experiments (Figure 5). In addition, SS inhibition was suppressed (Figures 6C–6E and 6L), suggesting that signals for both the 2nd SS peak and SS inhibition are processed at the SII. We also examined the effect of muscimol injections into the MI (Figures 6F–6J) because the 2nd SS peak was slightly increased by optical inactivation (Figures 5O and 5Q). The effects of MI muscimol injections on the 2nd SS peaks were not statistically significant (Figures 6H–6J and 6K). However, MI muscimol injections clearly suppressed the SS inhibition (Figures 6H–6J and 6L). Muscimol injections into the SI were

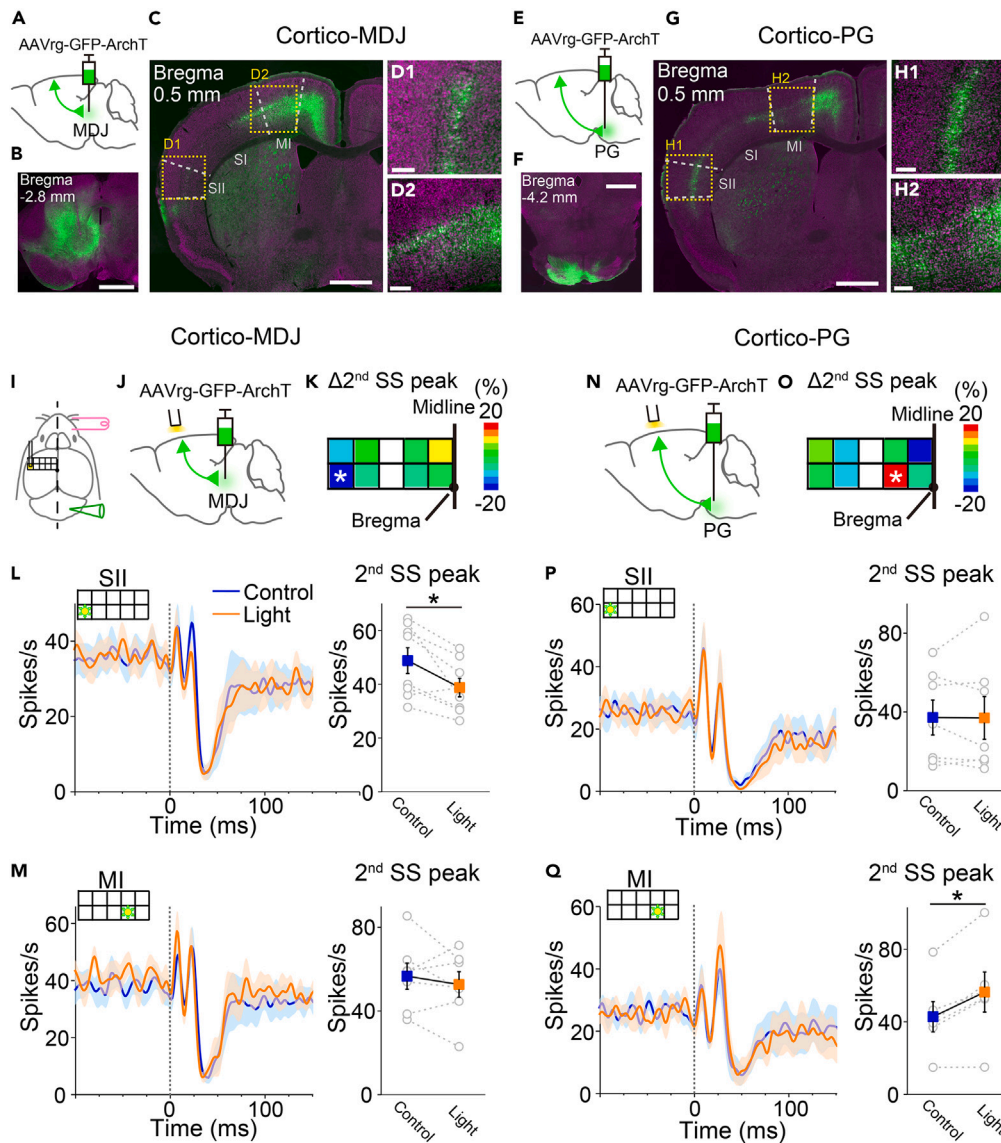


Figure 5. The 2nd SS peak is suppressed by optogenetic inactivation of the SII-MDJ, but not the cortico-PG pathway

(A and E) Schemas of injections of AAVrg-CamKII-ArchT-GFP, permitting retrograde expression of ArchT-GFP in projection neurons, into the MDJ (A) and the PG (E).
 (B and F) Fluorescent images of Nissl bodies (magenta) and GFP signals at AAV injection sites (green) in the MDJ (B) and PG (F). Scale bars; 1 mm.
 (C, D, G, H) Fluorescent images of Nissl bodies and GFP-labeled cortico-MDJ (C and D) and cortico-PG (G and H) neurons in the cerebral cortex at 0.5 mm rostral to the Bregma. Regions surrounded by dotted yellow lines in C and G are magnified in D and H, respectively. Scale bars; 1 mm (C and G) and 20 μ m (D and H).
 (I) Schema of ION stimulation (pink), SS recording (green) and optogenetic inactivation of cortical neurons. Yellow light (575 nm, 160 mW/mm²) was applied through a plastic optical fiber (0.4 mm diameter) that was placed in one of the grid columns.
 (J and N) Schemas of optical inactivation and AAV injection into the MDJ (J) and PG (N).
 (K and O) Pseudocolor coding of the average Δ 2nd SS peaks by light administration (see STAR Methods) onto cortico-MDJ (K) and cortico-PG (O) neurons. The grids marked with an asterisk indicate where the peak SS frequency with light illumination was significantly lower (K) or higher (O) than that without illumination (paired t-test, *p < 0.05). Number of trials used for calculating SDF for individual grids in individual PCs is 50. Number of PCs for individual grids are 5–8 (from 3 to 6 mice).

Figure 5. Continued

(L, M, P, Q) (Left) Peri-stimulus SDFs of SSs in response to right ION stimulation with (orange) or without (blue) 575 nm light illumination onto cortico–MDJ neurons in the SII (L; n = 8, from 6 mice) and MI (M; n = 7, from 6 mice) or cortico–PG neurons in the SII (P; n = 7, from 4 mice) and the MI (Q; n = 6, from 5 mice). Lines and shaded areas indicate mean and SEM, respectively. (Right) Changes in the 2nd SS peak induced by light illumination (paired t-test, *p < 0.05). Averaged data are presented as mean ± SEM. See also [Figures S1–S3](#) and [S6](#).

largely ineffective except at the lateral edge of the SI ([Figures 6K](#) and [6L](#)). These lines of evidence suggest that SS inhibition is processed by both the MI and SII.

Next, we investigated the mechanisms of SS inhibition. Muscimol injections suppressed the later and long inhibitory component (50 ms or later after ION stimulations) (the long inhibitory component) of the SS inhibition; however, the early and short component (~50 ms) (the short inhibitory component) was partially resistant ([Figures 1, 2, and 6](#)). This trend was more significant in the wide craniotomy experiment, which similarly suppressed the long inhibitory component, but not the short one ([Figure S2](#)). We conjectured that the SS inhibition was caused by overlapping short and long suppressing components mediated by distinct mechanisms. In the wide craniotomy experiments, both the 1st and 2nd SS peaks were preserved ([Figure S2](#)), but only the 1st SS peak was observed in the muscimol injection experiments ([Figures 1, 2, 6C, and 6D](#)). These data collectively suggest that the magnitude of the short inhibitory component is dependent on existence of the 1st and 2nd SS peaks. Because parallel fiber inputs activate inhibitory interneurons and suppress PC activity, we hypothesized that the short inhibitory component was mediated by feedforward inhibition. To test this, the surface of the Crus II was perfused with a GABA_A antagonist, SR95531 ([Figure S3A](#)). The local perfusion of SR95531 significantly reversed the short inhibitory component, within 50 ms of ION stimulation, but not the component after 50 ms ([Figures S3B and S3C](#)). These data suggest that the short inhibitory component is mediated by feedforward inhibition by cerebellar interneurons, likely driven by parallel fiber inputs.^{26,48}

DISCUSSION

In the present study, we locally injected muscimol into subcortical nuclei to block sensory signal transduction. To estimate the diffusion of muscimol, distances of individual injection sites from the center of 3D coordinates of effective cluster 4 ([Figures 3E–3H](#)) were calculated in the MDJ ([Figure S4](#)). Effective injection sites were mainly within 400 μm from the center of cluster 4. This estimation would be affected not only by muscimol diffusion but also by the size of the effective brain area and the total volume of injections. Therefore, it is likely that the muscimol diffusion distance is shorter than this estimation. Because distances between effective clusters in the MDJ, PG and PRNc were greater than 1 mm ([Figure 3H](#)), we infer that these areas are sufficiently separated from each other. However, muscimol injections into the MRN may also partially suppress the activities of neighboring nuclei, such as the nucleus of Darkschewitsch and interstitial nucleus of Cajal.

SS and complex spike generation have been reported to be suppressed by ketamine/xylazine.⁴⁹ However, the electrical ION stimulation and the air puff stimulation reproducibly evoked SSs ([Figures 1, 2, 4, 5, and 6](#)) and complex spikes³¹ under ketamine/xylazine anesthesia in our study, suggesting that PCs are capable of responding to ION and air puff stimulations. We examined the influence of anesthesia on the local field potential (LFP) in response to ION stimulation, which reflects network activity in the cerebellum. LFPs evoked by perioral stimulations are reported to have early and late components, termed T (trigeminal, peak latency ≈ 4.5 ms) and C (cortical, peak latency ≈ 16.1 ms) components in awake mice.²⁷ These components are similarly observed in anesthetized rats and mice.^{22–24,30} If signal transduction was severely perturbed by the anesthesia, the LFP waveform would be strongly changed. However, the LFP in our study had similar early and late components. Importantly, only the late component, which starts from around 15 ms after the stimulation and likely corresponds to the C component, was blocked by muscimol injections into the PG, MDJ or PRNc ([Figure S5](#)). These lines of evidence suggest that neuronal activity was sufficiently preserved to permit analysis of the signal transduction pathway in our experiment. However, it remains the possibility that the efficacy of sensory signal transduction via the cerebral cortex might be enhanced by ketamine/xylazine anesthesia.²³

Perioral sensory signals to the cerebellum are relayed by the indirect cortico–PG pathway via the PF and rostral MRN

The perioral sensory pathways for SS generation are summarized in [Figure S6](#). The signal transduction of the 1st SS peak was not suppressed by muscimol injections into the left cerebral cortex, MDJ, PG or PRNc

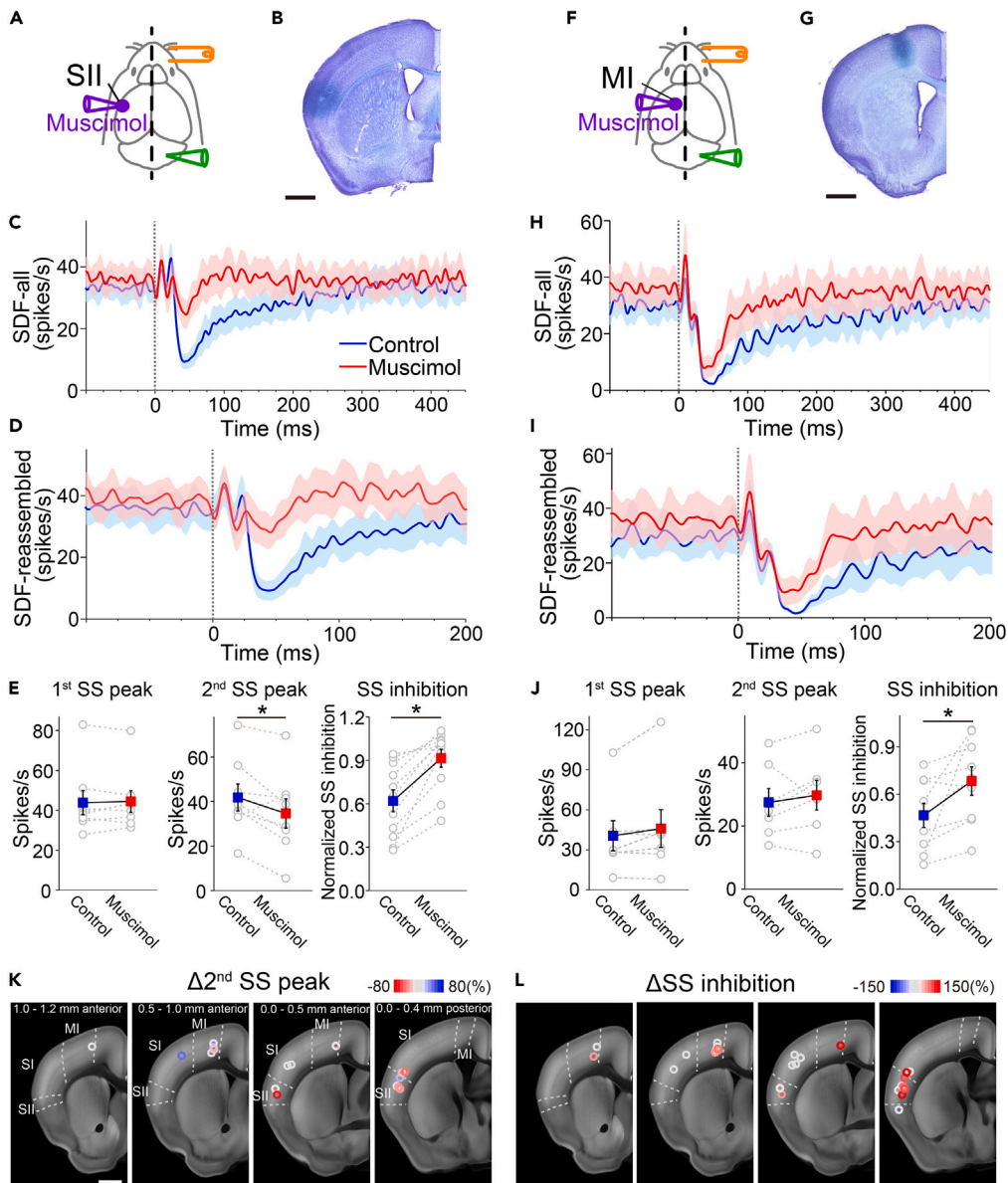


Figure 6. SS inhibition is relayed at both the SII and MI

(A and F) Schemas of ION stimulation (orange), recording (green) and muscimol injections (purple) into the left SI/SII (A) and MI (F).

(B and G) Muscimol injection sites in the SII (B) and MI (G).

(C and H) Peri-stimulus SDFs of SSs in response to right ION stimulation before (blue) and after (red) muscimol injections into the left SII (C) and MI (H). Data for all PCs (SII (C; n = 11, from 11 mice) and MI (H; n = 9, from 9 mice)) are presented. Lines and shaded areas indicate mean and SEM, respectively.

(D and I) Similar to C, H, but data for PCs with clear 1st and 2nd SS peaks (SII (D; n = 8, from 8 mice) and MI (I; n = 7, from 7 mice)) are presented.

(E and J) Changes in 1st SS peak (left), 2nd SS peak (middle) and normalized SS inhibition (right) produced by muscimol injections into the SII (E) and MI (J). The 1st and 2nd SS peaks are derived from reassembled data with clear peaks (D, I), and SS inhibitions are derived from all data (C, H). Paired t-test or Wilcoxon signed-rank test, *p < 0.05. Averaged data are presented as mean \pm SEM.

(K and L) Summary of centers of muscimol injection sites for $\Delta 2^{\text{nd}}$ SS peaks (K) and Δ SS inhibition (L) in the cerebral cortex. Injection sites were aligned to the Allen Mouse Common Coordinate Framework (CCFv3). Pseudocolor coding is as in Figure 1H. Scale bars: 1 mm (B, G, K). See also Figures S1 and S3–S6.

(Figures 1, 2 and 6), suggesting that it is mediated by the brainstem–cerebellar pathway, as reported previously.^{6,8,11–14,28} In contrast, the 2nd SS peak and SS inhibition were transmitted via the cortical route (Figure S6). The optical inactivation and muscimol injection experiments collectively suggest that the signals mediated by the 2nd SS peak are transmitted by the SII–MDJ pathway, but not by cortico–PG pathways (Figures 5, 6, and S6). The cortical area sensitive to these manipulations comprised the SII and the lateral edge of the SI, according to the Allen Mouse Common Coordinate Framework (CCFv3) (Figures 5 and 6). This area is near the SI upper lip region that was reported to relay perioral sensory signals to the cerebellum.²³

SS inhibition was shortened by muscimol injections into both the SII and MI (Figure 6), suggesting that the signals for SS inhibition are processed by relatively broad cortical areas (Figure S6). This finding suggests that signals for the 2nd SS peak and the SS inhibition might be differentially processed in the cerebral cortex. However, these sensory signals are likely transmitted to the MDJ, because they are similarly suppressed by muscimol injections into the MDJ and PG (Figures 1, 2, and 3). We could not identify the output pathway for the SS inhibition from the cerebral cortex because of the experimental limitation (Figure S2). Meanwhile, we found that the 2nd SS peak was slightly enhanced by optogenetic inactivation of the cortico–PG neurons in the MI (Figures 5O and 5Q), suggesting that the MI neurons that project to the PG may, at least partly, participate in signal transduction for the SS inhibition. The SS inhibition may be processed by interconnections between the SII and MI,^{50–52} and subsequently transmitted to the MDJ. A contribution by this pathway might explain why the SS inhibition was more susceptible to the wide craniotomy (Figure S2). Alternatively, signals from the MI–PG neurons may be transmitted to the MDJ via collaterals to the thalamic and midbrain areas,³⁵ which might recruit inhibitory neurons in the zona incerta^{33,53} and/or MRN⁵⁴ and affect signal transduction. Guo et al. reported the polysynaptic inhibition of PG neurons by the motor cortex.¹⁵ Interestingly, it has been reported that MI activation also suppresses sensory signal transduction via the inferior olive–climbing fiber–PC pathway.^{31,55} Sensory signaling to the cerebellum may therefore be generally subject to inhibitory regulation by the motor cortex.

Our findings suggest that SS inhibition consists of short and long inhibitory components, and that the short component is likely mediated by feedforward inhibition by cerebellar interneurons. In contrast, the mechanisms underlying the long inhibitory component are currently unclear. SIs are reported to be suppressed by generation of complex spikes (SS pause).⁵⁶ Because muscimol injections into the MDJ reduced the complex spikes evoked by ION stimulation,³¹ the reduced SS inhibition by muscimol may be attributable to the reduced SS pause. However, the SS inhibition was not affected by the presence or absence of complex spikes in the present study (Figures S3D and S3E), suggesting that reduction of the complex spike is not a major cause of the suppression of SS inhibition.²⁵ Transmission of the sensory signal may be inhibited *en route* to the cerebellum. Similar long inhibition of spike firing is also observed in the Golgi cells in the Crus I/II after tactile stimulation.⁵⁷ Because both Purkinje cells and Golgi cells share inputs from the mossy fiber–granule cell–parallel fiber pathway, such long firing inhibition may be caused by suppression of sensory inputs *en route* to the cerebellum.

The PG is one of the major sources of mossy fibers,^{6,8,11–14} and receives monosynaptic cortico–PG projections from the entire cerebral cortex in a topographically organized fashion.^{4–10} Most previous studies assumed that signal transduction from the cerebral cortex to the PG is mediated by the monosynaptic cortico–PG pathway. However, the present findings suggest that the perioral sensory signal is transmitted to the cerebellum by the indirect cortico–PG pathway, but not by the monosynaptic cortico–PG pathway (Figure S6). The area around the PF and MRN in the MDJ is not a source of mossy fibers,^{45,46} and the MDJ and PG are in series in the signaling pathway (Figures 2M–2Q). In addition, the PG is the major source of the mossy fibers projecting to the cerebellum. These observations collectively suggest that the MDJ relays sensory signals to the PG. However, the signaling pathway from the MDJ to the PG remains unclear. Fluorogold injection into the PG retrogradely stained neurons in the MDJ (Figure S7), suggesting the presence of the direct MDJ–PG projection, as reported previously.^{37–40} This direct projection may participate in sensory signal transduction. This point should be addressed in the future studies.

In the present study, we cannot exclude the existence of sensory transduction pathways originating from other cortical areas because we mainly focused on the cortical areas around motor and somatosensory areas based on previous experiments.²³ Thus, sensory signals might be relayed by areas not experimentally manipulated in the current study. Morissette et al. reported that suppression of the C component of the LFP

by local SI inhibition (by lidocaine administration or ablation) is milder than that produced by decerebration, which totally eliminates signal transduction from the forebrain and midbrain.³⁰ This suggests the existence of other minor pathways that are not relayed at the somatosensory area, but participate in sensory signal transduction to the cerebellum. The monosynaptic cortico–pontine pathway originating from untested cortical areas may also participate in signal transduction.

Cortico–cerebellar sensory transduction may be processed by reticular formation networks

In the present study, muscimol injections into the PRNc also effectively suppressed the 2nd SS peak and SS inhibition (Figures 2 and 3). However, it is currently unclear how the PRNc is involved in perioral signal transmission. The PRNc has projections to the pontine tegmental reticular nucleus adjacent to the PG but sparse to the PG (Figure S7)³⁸ (Allen Mouse Brain Connectivity Atlas: <https://connectivity.brain-map.org/projection/experiment/158838128>).⁴¹ Furthermore, the projections from the SII or MI to the PRNc is very sparse comparing to those to the MDJ (Allen Mouse Brain Connectivity Atlas: <https://connectivity.brain-map.org/projection/experiment/117298988> (SII) or <https://connectivity.brain-map.org/projection/experiment/127084296> (MI)). Together, these results suggest that the PRNc may not be directly involved in the perioral sensory transduction pathway. We hypothesize that the PRNc contributes to signal transduction through reciprocal connections with the MDJ (Figure S6). Previous reports demonstrate that mesencephalic, pontine and medullary reticular formations form reciprocal projections with each other.^{33,38,58,59} Some reciprocal connections may form a local circuit that acts as a functional unit for processing sensory signals. Future studies should clarify the functional roles of the reticular formation networks.

Previous reports have demonstrated that integration of multimodal information originating from different cortical areas occurs in the various stages of signal transduction to the cerebellum.^{17,60–62} Some PG neurons are reported to be activated by the polymodal sensory response^{15,63} and by stimulation of various cortical areas^{63,64} (however, see⁶⁵). Neurons in the reticular formation can be activated by different sensory inputs, such as somatosensory, auditory, olfactory and visual signals, with some neurons responsive to polymodal inputs.^{66–70} Reticular formation networks may participate in the integration and preprocessing of multimodal sensory signals conveyed to the cerebellum.

Limitations of the study

- Owing to unexpected suppression of the SS inhibition by broad craniotomy, signaling pathways for the SS inhibition from the cerebral cortex remain unclear. Functional roles of the MI–SII cortical connections and collateral projections to the MDJ in SS inhibition should be addressed in future studies.
- The signaling pathway from the MDJ to the PG is still unclear. We confirmed the existence of the direct anatomical projections from the MDJ to the PG reported previously, but the functional contribution of this direct pathway needs to be addressed in future studies.
- The input and output pathways for the PRNc remain unclear. The connections among the reticular formations, as well as their functional roles, need to be clarified in future studies.

STAR★METHODS

Detailed methods are provided in the online version of this paper and include the following:

- KEY RESOURCES TABLE
- RESOURCE AVAILABILITY
 - Lead contact
 - Materials availability
 - Data and code availability
- EXPERIMENTAL MODEL AND STUDY PARTICIPANT DETAILS
 - Mice
- METHOD DETAILS
 - *In vivo* single unit recording
 - Muscimol injections
 - Virus injections
 - Optogenetics
 - GABA_AR blocker perfusion
 - Retrograde tracer injections

- Histological analysis
- Hierarchical clustering analysis
- **QUANTIFICATION AND STATISTICAL ANALYSIS**

SUPPLEMENTAL INFORMATION

Supplemental information can be found online at <https://doi.org/10.1016/j.isci.2023.107301>.

ACKNOWLEDGMENTS

This work was supported by Grants-in-Aid for Scientific Research (19K16278, 21H05695 and 22K15227 to R.K.; 16K10182, 17KK0161 and 20K07938 to T.Y.; and 22K19362 to K.H.) from MEXT Japan. This work was also supported by AMED under Grant Number JP23gm6510017 to K.H. We thank Barry Patel, PhD, from Edanz (<https://jp.edanz.com/ac>), for editing a draft of this manuscript.

AUTHOR CONTRIBUTIONS

RK: Conceptualization, Methodology, Validation, Formal analysis, Investigation, Data curation, Writing – original draft, Writing – Review and Editing, Visualization, Funding acquisition. TY: Methodology, Validation, Investigation, Resource, Data curation, Writing – Review and Editing, Funding acquisition. KY: Methodology, Validation, Investigation, Data curation, Writing – Review & Editing. KH: Conceptualization, Methodology, Validation, Formal analysis, Investigation, Data curation, Writing – original draft, Writing – Review and Editing, Visualization, Supervision, Project administration, Funding acquisition.

DECLARATION OF INTERESTS

The authors declare no competing interests.

INCLUSION AND DIVERSITY

We support inclusive, diverse, and equitable conduct of research.

Received: February 16, 2023

Revised: May 26, 2023

Accepted: July 3, 2023

Published: July 11, 2023

REFERENCES

1. Allen, G.I., and Tsukahara, N. (1974). Cerebrocerebellar communication systems. *Physiol. Rev.* 54, 957–1006. <https://doi.org/10.1152/physrev.1974.54.4.957>.
2. Ito, M. (2012). *The Cerebellum* (FT Press).
3. Schmahmann, J.D. (1998). Dysmetria of thought: clinical consequences of cerebellar dysfunction on cognition and affect. *Trends Cognit. Sci.* 2, 362–371. [https://doi.org/10.1016/s1364-6613\(98\)01218-2](https://doi.org/10.1016/s1364-6613(98)01218-2).
4. Henschke, J.U., and Pakan, J.M. (2020). Disynaptic cerebrocerebellar pathways originating from multiple functionally distinct cortical areas. *Elife* 9, e59148. <https://doi.org/10.7554/eLife.59148>.
5. Leergaard, T.B., and Bjaalie, J.G. (2007). Topography of the complete corticopontine projection: from experiments to principal Maps. *Front. Neurosci.* 1, 211–223. <https://doi.org/10.3389/neuro.01.1.1.016.2007>.
6. Leergaard, T.B., Lillehaug, S., De Schutter, E., Bower, J.M., and Bjaalie, J.G. (2006). Topographical organization of pathways from somatosensory cortex through the pontine nuclei to tactile regions of the rat cerebellar hemispheres. *Eur. J. Neurosci.* 24, 2801–2812. <https://doi.org/10.1111/j.1460-9568.2006.05150.x>.
7. Mihailoff, G.A., Lee, H., Watt, C.B., and Yates, R. (1985). Projections to the basilar pontine nuclei from face sensory and motor regions of the cerebral cortex in the rat. *J. Comp. Neurol.* 237, 251–263. <https://doi.org/10.1002/cne.902370209>.
8. Odeh, F., Ackerley, R., Bjaalie, J.G., and Apps, R. (2005). Pontine maps linking somatosensory and cerebellar cortices are in register with climbing fiber somatotopy. *J. Neurosci.* 25, 5680–5690. <https://doi.org/10.1523/JNEUROSCI.0558-05.2005>.
9. Panto, M.R., Cicerata, F., Angaut, P., Parenti, R., and Serapide, F. (1995). The projection from the primary motor and somatic sensory cortex to the basilar pontine nuclei. A detailed electrophysiological and anatomical study in the rat. *J. Hirnforsch.* 36, 7–19.
10. Legg, C.R., Mercier, B., and Glickstein, M. (1989). Corticopontine projection in the rat: the distribution of labelled cortical cells after large injections of horseradish peroxidase in the pontine nuclei. *J. Comp. Neurol.* 286, 427–441. <https://doi.org/10.1002/cne.902860403>.
11. Biswas, M.S., Luo, Y., Sarpong, G.A., and Sugihara, I. (2019). Divergent projections of single pontocerebellar axons to multiple cerebellar lobules in the mouse. *J. Comp. Neurol.* 527, 1966–1985. <https://doi.org/10.1002/cne.24662>.
12. Mihailoff, G.A., Burne, R.A., Azizi, S.A., Norell, G., and Woodward, D.J. (1981). The pontocerebellar system in the rat: an HRP study. II. Hemispherical components. *J. Comp. Neurol.* 197, 559–577. <https://doi.org/10.1002/cne.901970403>.
13. Pijpers, A., and Ruigrok, T.J.H. (2006). Organization of pontocerebellar projections to identified climbing fiber zones in the rat. *J. Comp. Neurol.* 496, 513–528. <https://doi.org/10.1002/cne.20940>.
14. Serapide, M.F., Panto, M.R., Parenti, R., Zappalá, A., and Cicerata, F. (2001). Multiple zonal projections of the basilar pontine nuclei to the cerebellar cortex of the rat. *J. Comp. Neurol.* 430, 471–484. [https://doi.org/10.1002/1096-9861\(20010219\)430:4<471::aid-cne1044>3.0.co;2-g](https://doi.org/10.1002/1096-9861(20010219)430:4<471::aid-cne1044>3.0.co;2-g).

15. Guo, J.Z., Sauerbrei, B.A., Cohen, J.D., Mischiati, M., Graves, A.R., Pisanello, F., Branson, K.M., and Hantman, A.W. (2021). Disrupting cortico-cerebellar communication impairs dexterity. *Elife* 10, e65906. <https://doi.org/10.7554/eLife.65906>.
16. Matsunami, K. (1987). Neuronal activity in nuclei pontis and reticularis tegmenti pontis related to forelimb movements of the monkey. *Neurosci. Res.* 5, 140–156. [https://doi.org/10.1016/0168-0102\(87\)90030-7](https://doi.org/10.1016/0168-0102(87)90030-7).
17. Rüegg, D., and Wiesendanger, M. (1975). Corticofugal effects from sensorimotor area I and somatosensory area II on neurones of the pontine nuclei in the cat. *J. Physiol.* 247, 745–757. <https://doi.org/10.1113/jphysiol.1975.sp010955>.
18. Suzuki, D.A., May, J.G., Keller, E.L., and Yee, R.D. (1990). Visual motion response properties of neurons in dorsolateral pontine nucleus of alert monkey. *J. Neurophysiol.* 63, 37–59. <https://doi.org/10.1152/jn.1990.63.1.37>.
19. Thier, P., Koehler, W., and Buettner, U.W. (1988). Neuronal activity in the dorsolateral pontine nucleus of the alert monkey modulated by visual stimuli and eye movements. *Exp. Brain Res.* 70, 496–512. <https://doi.org/10.1007/BF00247598>.
20. Tziridis, K., Dicke, P.W., and Thier, P. (2009). The role of the monkey dorsal pontine nuclei in goal-directed eye and hand movements. *J. Neurosci.* 29, 6154–6166. <https://doi.org/10.1523/JNEUROSCI.0581-09.2009>.
21. Wagner, M.J., Kim, T.H., Kadmon, J., Nguyen, N.D., Ganguli, S., Schnitzer, M.J., and Luo, L. (2019). Shared Cortex-Cerebellum Dynamics in the Execution and Learning of a Motor Task. *Cell* 177, 669–682.e24. <https://doi.org/10.1016/j.cell.2019.02.019>.
22. Brown, I.E., and Bower, J.M. (2001). Congruence of mossy fiber and climbing fiber tactile projections in the lateral hemispheres of the rat cerebellum. *J. Comp. Neurol.* 429, 59–70.
23. Shimuta, M., Sugihara, I., and Ishikawa, T. (2020). Multiple signals evoked by unisensory stimulation converge onto cerebellar granule and Purkinje cells in mice. *Commun. Biol.* 3, 381. <https://doi.org/10.1038/s42003-020-1110-2>.
24. Tahon, K., Wijnants, M., De Schutter, E., and Maex, R. (2011). Current source density correlates of cerebellar Golgi and Purkinje cell responses to tactile input. *J. Neurophysiol.* 105, 1327–1341. <https://doi.org/10.1152/jn.00317.2010>.
25. Bosman, L.W.J., Koekkoek, S.K.E., Shapiro, J., Rijken, B.F.M., Zandstra, F., van der Ende, B., Owens, C.B., Potters, J.W., de Gruij, J.R., Ruigrok, T.J.H., and De Zeeuw, C.I. (2010). Encoding of whisker input by cerebellar Purkinje cells. *J. Physiol.* 588, 3757–3783. <https://doi.org/10.1113/jphysiol.2010.195180>.
26. Chu, C.P., Bing, Y.H., and Qiu, D.L. (2011). Sensory stimulus evokes inhibition rather than excitation in cerebellar Purkinje cells *in vivo* in mice. *Neurosci. Lett.* 487, 182–186. <https://doi.org/10.1016/j.neulet.2010.10.018>.
27. Márquez-Ruiz, J., and Cheron, G. (2012). Sensory stimulation-dependent plasticity in the cerebellar cortex of alert mice. *PLoS One* 7, e36184. <https://doi.org/10.1371/journal.pone.0036184>.
28. Woolston, D.C., Kassel, J., and Gibson, J.M. (1981). Trigemino-cerebellar mossy fiber branching to granule cell layer patches in the rat cerebellum. *Brain Res.* 209, 255–269. [https://doi.org/10.1016/0006-8993\(81\)90152-9](https://doi.org/10.1016/0006-8993(81)90152-9).
29. Kennedy, T.T., Grimm, R.J., and Towe, A.L. (1966). The role of cerebral cortex in evoked somatosensory activity in cat cerebellum. *Exp. Neurol.* 14, 13–32. [https://doi.org/10.1016/0014-4886\(66\)90021-5](https://doi.org/10.1016/0014-4886(66)90021-5).
30. Morissette, J., and Bower, J.M. (1996). Contribution of somatosensory cortex to responses in the rat cerebellar granule cell layer following peripheral tactile stimulation. *Exp. Brain Res.* 109, 240–250. <https://doi.org/10.1007/BF00231784>.
31. Kubo, R., Aiba, A., and Hashimoto, K. (2018). The anatomical pathway from the mesodiencephalic junction to the inferior olive relays perioral sensory signals to the cerebellum in the mouse. *J. Physiol.* 596, 3775–3791. <https://doi.org/10.1113/JP275836>.
32. Carlton, S.M., Leichnetz, G.R., and Mayer, J.D. (1982). Projections from the nucleus parafascicularis pruberualis to medullary raphe nuclei and inferior olive in the rat: a horseradish peroxidase and autoradiography study. *Neurosci. Lett.* 30, 191–197.
33. Shammah-Lagnado, S.J., Ricardo, J.A., Sakamoto, N.T., and Negrão, N. (1983). Afferent connections of the mesencephalic reticular formation: a horseradish peroxidase study in the rat. *Neuroscience* 9, 391–409. [https://doi.org/10.1016/0306-4522\(83\)90302-0](https://doi.org/10.1016/0306-4522(83)90302-0).
34. Stuesse, S.L., and Newman, D.B. (1990). Projections from the medial agranular cortex to brain stem visuomotor centers in rats. *Exp. Brain Res.* 80, 532–544.
35. Muñoz-Castañeda, R., Zingg, B., Matho, K.S., Chen, X., Wang, Q., Foster, N.N., Li, A., Narasimhan, A., Hirokawa, K.E., Huo, B., et al. (2021). Cellular anatomy of the mouse primary motor cortex. *Nature* 598, 159–166. <https://doi.org/10.1038/s41586-021-03970-w>.
36. Wang, X., Novello, M., Gao, Z., Ruigrok, T.J.H., and De Zeeuw, C.I. (2022). Input and output organization of the mesodiencephalic junction for cerebro-cerebellar communication. *J. Neurosci. Res.* 100, 620–637. <https://doi.org/10.1002/jnr.24993>.
37. Aas, J.E., and Brodal, P. (1990). GABA and glycine as putative transmitters in subcortical pathways to the pontine nuclei. A combined immunocytochemical and retrograde tracing study in the cat with some observations in the rat. *Neuroscience* 34, 149–162. [https://doi.org/10.1016/0306-4522\(90\)90309-r](https://doi.org/10.1016/0306-4522(90)90309-r).
38. Jones, B.E., and Yang, T.Z. (1985). The efferent projections from the reticular formation and the locus coeruleus studied by anterograde and retrograde axonal transport in the rat. *J. Comp. Neurol.* 242, 56–92. <https://doi.org/10.1002/cne.902420105>.
39. Mihailoff, G.A., Kosinski, R.J., Azizi, S.A., and Border, B.G. (1989). Survey of noncortical afferent projections to the basilar pontine nuclei: a retrograde tracing study in the rat. *J. Comp. Neurol.* 282, 617–643. <https://doi.org/10.1002/cne.902820411>.
40. Khalil, A.J., Mansvelter, H.D., and Witter, L. (2022). Mesodiencephalic junction GABAergic inputs are processed separately from motor cortical inputs in the basilar pons. *iScience* 25, 104641. <https://doi.org/10.1016/j.isci.2022.104641>.
41. Oh, S.W., Harris, J.A., Ng, L., Winslow, B., Cain, N., Mihalas, S., Wang, Q., Lau, C., Kuan, L., Henry, A.M., et al. (2014). A mesoscale connectome of the mouse brain. *Nature* 508, 207–214. <https://doi.org/10.1038/nature13186>.
42. Wang, Q., Ding, S.L., Li, Y., Royall, J., Feng, D., Lesnar, P., Graddis, N., Naeemi, M., Facer, B., Ho, A., et al. (2020). The Allen Mouse Brain Common Coordinate Framework: A 3D Reference Atlas. *Cell* 181, 936–953.e20. <https://doi.org/10.1016/j.cell.2020.04.007>.
43. Lein, E.S., Hawrylycz, M.J., Ao, N., Ayres, M., Bensinger, A., Bernard, A., Boe, A.F., Boguski, M.S., Brockway, K.S., Byrnes, E.J., et al. (2007). Genome-wide atlas of gene expression in the adult mouse brain. *Nature* 445, 168–176. <https://doi.org/10.1038/nature05453>.
44. Vogt, N. (2020). The mouse reference brain in 3D. *Nat. Methods* 17, 655. <https://doi.org/10.1038/s41592-020-0899-4>.
45. Altman, J., and Bayer, S.A. (1996). *Development of the Cerebellar System: In Relation to its Evolution, Structure, and Functions* (CRC press, Inc.).
46. Fu, Y., Tvrdik, P., Makki, N., Paxinos, G., and Watson, C. (2011). Precerebellar cell groups in the hindbrain of the mouse defined by retrograde tracing and correlated with cumulative Wnt1-cre genetic labeling. *Cerebellum* 10, 570–584. <https://doi.org/10.1007/s12311-011-0266-1>.
47. Economo, M.N., Viswanathan, S., Tasic, B., Bas, E., Winnubst, J., Menon, V., Graybiuck, L.T., Nguyen, T.N., Smith, K.A., Yao, Z., et al. (2018). Distinct descending motor cortex pathways and their roles in movement. *Nature* 563, 79–84. <https://doi.org/10.1038/s41586-018-0642-9>.
48. Chu, C.P., Bing, Y.H., Liu, Q.R., and Qiu, D.L. (2011). Synaptic responses evoked by tactile stimuli in Purkinje cells in mouse cerebellar cortex Crus II *in vivo*. *PLoS One* 6, e22752. <https://doi.org/10.1371/journal.pone.0022752>.
49. Bengtsson, F., and Jörntell, H. (2007). Ketamine and xylazine depress sensory-evoked parallel fiber and climbing fiber

- responses. *J. Neurophysiol.* 98, 1697–1705. <https://doi.org/10.1152/jn.00057.2007>.
50. Miyashita, E., Keller, A., and Asanuma, H. (1994). Input-output organization of the rat vibrissal motor cortex. *Exp. Brain Res.* 99, 223–232. <https://doi.org/10.1007/BF00239589>.
 51. Colechio, E.M., and Alloway, K.D. (2009). Differential topography of the bilateral cortical projections to the whisker and forepaw regions in rat motor cortex. *Brain Struct. Funct.* 213, 423–439. <https://doi.org/10.1007/s00429-009-0215-7>.
 52. Reep, R.L., Goodwin, G.S., and Corwin, J.V. (1990). Topographic organization in the corticocortical connections of medial agranular cortex in rats. *J. Comp. Neurol.* 294, 262–280. <https://doi.org/10.1002/cne.902940210>.
 53. Mihailoff, G.A. (1995). Orthograde axonal transport studies of projections from the zona incerta and pretegmentum to the basilar pontine nuclei in the rat. *J. Comp. Neurol.* 360, 301–318. <https://doi.org/10.1002/cne.903600208>.
 54. Border, B.G., Kosinski, R.J., Azizi, S.A., and Mihailoff, G.A. (1986). Certain basilar pontine afferent systems are GABA-ergic: combined HRP and immunocytochemical studies in the rat. *Brain Res. Bull.* 17, 169–179. [https://doi.org/10.1016/0361-9230\(86\)90113-9](https://doi.org/10.1016/0361-9230(86)90113-9).
 55. Leicht, R., Rowe, M.J., and Schmidt, R.F. (1973). Cortical and peripheral modification of cerebellar climbing fibre activity arising from cutaneous mechanoreceptors. *J. Physiol.* 228, 619–635.
 56. Tang, T., Xiao, J., Suh, C.Y., Burroughs, A., Cerminara, N.L., Jia, L., Marshall, S.P., Wise, A.K., Apps, R., Sugihara, I., and Lang, E.J. (2017). Heterogeneity of Purkinje cell simple spike-complex spike interactions: zebrin- and non-zebrin-related variations. *J. Physiol.* 595, 5341–5357. <https://doi.org/10.1113/JP274252>.
 57. Vos, B.P., Volny-Luraghi, A., and De Schutter, E. (1999). Cerebellar Golgi cells in the rat: receptive fields and timing of responses to facial stimulation. *Eur. J. Neurosci.* 11, 2621–2634. <https://doi.org/10.1046/j.1460-9568.1999.00678.x>.
 58. Shammah-Lagnado, S.J., Negrão, N., Silva, B.A., and Ricardo, J.A. (1987). Afferent connections of the nuclei reticularis pontis oralis and caudalis: a horseradish peroxidase study in the rat. *Neuroscience* 20, 961–989. [https://doi.org/10.1016/0306-4522\(87\)90256-9](https://doi.org/10.1016/0306-4522(87)90256-9).
 59. Veazey, R.B., and Severin, C.M. (1980). Efferent projections of the deep mesencephalic nucleus (pars medialis) in the rat. *J. Comp. Neurol.* 190, 245–258. <https://doi.org/10.1002/cne.901900204>.
 60. Huang, C.C., Sugino, K., Shima, Y., Guo, C., Bai, S., Mensh, B.D., Nelson, S.B., and Hantman, A.W. (2013). Convergence of pontine and proprioceptive streams onto multimodal cerebellar granule cells. *Elife* 2, e00400. <https://doi.org/10.7554/eLife.00400>.
 61. Ishikawa, T., Shimuta, M., and Häusser, M. (2015). Multimodal sensory integration in single cerebellar granule cells *in vivo*. *Elife* 4, e12916. <https://doi.org/10.7554/eLife.12916>.
 62. Proville, R.D., Spolidoro, M., Guyon, N., Dugué, G.P., Selimi, F., Isope, P., Popa, D., and Léna, C. (2014). Cerebellum involvement in cortical sensorimotor circuits for the control of voluntary movements. *Nat. Neurosci.* 17, 1233–1239. <https://doi.org/10.1038/nn.3773>.
 63. Boyd, J., and Aitkin, L. (1976). Responses of single units in the pontine nuclei of the cat to acoustic stimulation. *Neurosci. Lett.* 3, 259–263. [https://doi.org/10.1016/0304-3940\(76\)90052-5](https://doi.org/10.1016/0304-3940(76)90052-5).
 64. Potter, R.F., Rüegg, D.G., and Wiesendanger, M. (1978). Responses of neurones of the pontine nuclei to stimulation of the sensorimotor, visual and auditory cortex of rats. *Brain Res. Bull.* 3, 15–19. [https://doi.org/10.1016/0361-9230\(78\)90056-4](https://doi.org/10.1016/0361-9230(78)90056-4).
 65. Baker, J., Gibson, A., Glickstein, M., and Stein, J. (1976). Visual cells in the pontine nuclei of the cat. *J. Physiol.* 255, 415–433. <https://doi.org/10.1113/jphysiol.1976.sp011287>.
 66. Bell, C., Sierra, G., Buendia, N., and Segundo, J.P. (1964). Sensory Properties of Neurons in the Mesencephalic Reticular Formation. *J. Neurophysiol.* 27, 961–987. <https://doi.org/10.1152/jn.1964.27.6.961>.
 67. Groves, P.M., Miller, S.W., Parker, M.V., and Rebec, G.V. (1973). Organization by sensory modality in the reticular formation of the rat. *Brain Res.* 54, 207–224. [https://doi.org/10.1016/0006-8993\(73\)90045-0](https://doi.org/10.1016/0006-8993(73)90045-0).
 68. Irvine, D.R., and Jackson, G.D. (1983). Auditory input to neurons in mesencephalic and rostral pontine reticular formation: an electrophysiological and horseradish peroxidase study in the cat. *J. Neurophysiol.* 49, 1319–1333. <https://doi.org/10.1152/jn.1983.49.6.1319>.
 69. Motokizawa, F. (1974). Electrophysiological studies of olfactory projection to the mesencephalic reticular formation. *Exp. Neurol.* 44, 135–144. [https://doi.org/10.1016/0014-4886\(74\)90054-5](https://doi.org/10.1016/0014-4886(74)90054-5).
 70. Siegel, J.M. (1979). Behavioral functions of the reticular formation. *Brain Res.* 180, 69–105. [https://doi.org/10.1016/0165-0173\(79\)90017-1](https://doi.org/10.1016/0165-0173(79)90017-1).
 71. Han, X., Chow, B.Y., Zhou, H., Klapoetke, N.C., Chuong, A., Rajimehr, R., Yang, A., Baratta, M.V., Winkle, J., Desimone, R., and Boyden, E.S. (2011). A high-light sensitivity optical neural silencer: development and application to optogenetic control of non-human primate cortex. *Front. Syst. Neurosci.* 5, 18. <https://doi.org/10.3389/fnsys.2011.00018>.
 72. Shamash, P., Carandini, M., Harris, K., and Steinmetz, N. (2018). A tool for analyzing electrode tracks from slice histology. Preprint at bioRxiv. <https://doi.org/10.1101/447995>.

STAR★METHODS

KEY RESOURCES TABLE

| REAGENT or RESOURCE | SOURCE | IDENTIFIER |
|--|---|---|
| Bacterial and virus strains | | |
| pAAV-CamKII-ArchT-GFP (PV2527) | Han et al. ⁷¹ | Addgene 99039-AAVrg |
| Chemicals, peptides, and recombinant proteins | | |
| ketamine | Daiichi Sankyo | S0-018923 |
| Xylazine | Elanco Japan | selactar |
| muscimol | Tocris Bioscience | Cat#0289; CAS#2763-96-4 |
| Chicago Sky Blue 6B | Sigma-Aldrich | C8679; CAS#2610-05-1 |
| SR95531 | Tocris Bioscience | Cat#1262; CAS#104104-50-9 |
| Fluoro-Gold | Wako | 52-9400 |
| Cresyl violet solution | MUTO | 41022 |
| NeuroTrace 500/525 Green Fluorescent Nissl Stain | Thermo Fisher Scientific | N21480 |
| NeuroTrace 530/615 Red Fluorescent Nissl Stain | Thermo Fisher Scientific | N21482 |
| Deposited data | | |
| ALLEN BRAIN ATLAS | https://atlas.brain-map.org/ | |
| Allen Mouse Brain Connectivity Atlas | connectivity.brain-map.org/projection/experiment/158838128 | |
| Allen Mouse Brain Connectivity Atlas | connectivity.brain-map.org/projection/experiment/117298988 | |
| Allen Mouse Brain Connectivity Atlas | connectivity.brain-map.org/projection/experiment/127084296 | |
| Experimental models: Organisms/strains | | |
| Mouse: C57BL/6J | CREA Japan | C57BL/6Jcl |
| Software and algorithms | | |
| Axograph X | Axograph Scientific | https://axograph.com/ |
| OriginPro | LightStone | https://www.lightstone.co.jp/origin/ |
| MATLAB | MathWorks | https://jp.mathworks.com/products/matlab.html |
| SigmaPlot 12.5 | Systat Software | RRID: SCR_010285 |
| Other | | |
| Multiclamp 700B | Molecular Devices | N/A |
| SPECTRA X Light Engine | Lumencor | N/A |
| Nanoject II Auto-Nanoliter Injector | Drummond | N/A |
| HS All-in-one Fluorescence Microscope | KEYENCE | BZ-9000 |

RESOURCE AVAILABILITY

Lead contact

Further information and requests for resources and reagents should be directed to and will be fulfilled by the lead contact, Kouichi Hashimoto (hashik@hiroshima-u.ac.jp).

Materials availability

This study did not generate any new unique reagents.

Data and code availability

- All original data reported in this paper will be shared by the [lead contact](#) upon request. This paper partly uses existing, publicly available data. Accession websites are listed in the [key resources table](#).
- This paper does not report original code.
- Any additional information required to reanalyze the data reported in this paper is available from the [lead contact](#) upon request.

EXPERIMENTAL MODEL AND STUDY PARTICIPANT DETAILS

Mice

All animal experiments were performed in accordance with guidelines from the Animal Research Committee (#A23-39) and the biosafety committee for living modified organisms (#2023-35) of Hiroshima University. Male C57BL/6J mice at approximately postnatal day 60–90 were used in all experiments. C57BL/6J mice were obtained from CREA Japan. All mice were provided with water and food *ad libitum*, and were maintained under specific pathogen-free conditions on a 12/12-h light/dark cycle (lights on at 08:00 a.m.) at constant room temperature ($23 \pm 2^\circ\text{C}$) and humidity (60%). Littermates were randomly assigned to experimental groups.

METHOD DETAILS

In vivo single unit recording

Animals were anesthetized by intraperitoneal injection of a mixture of ketamine (100 mg/kg; Daiichi Sankyo, Japan) and xylazine (10 mg/kg; Elanco Japan, Japan). The depth of anesthesia was monitored by vibrissae movements. Under deep anesthesia, ION stimulation induced movement of the mystacial pad only on the ipsilateral side, without sporadic movements. When sporadic whisker movements were detected or both sides of the mystacial pad were simultaneously moved by stimulation to one side of the ION, a mixture of ketamine (13 mg/ml) and xylazine (1.3 mg/ml) was administered from a cannula with a needle inserted into the hind limb muscles. This anesthetic mixture was administered at approximately 40 μl per injection, until the contralateral mystacial pad movement stopped. The total supplemental volume of the mixture did not exceed 200 μl . Body temperature was maintained at $37 \pm 1^\circ\text{C}$ using a heating pad (FHC, USA). After reaching a surgical level of anesthesia, the animal's head was fixed in a stereotaxic apparatus (Narishige, Japan), an incision was made in the skin, and the skull over the right cerebellum was exposed by removing the muscles and connective tissues. Lidocaine gel (AstraZeneca, UK) was applied to the skin incision. A craniotomy (2–3 mm in diameter) was performed using a micro-drill (Nakanishi, Japan) at approximately 3.5 mm lateral from the midline on the occipital bone over a right cerebellar folium (Crus II). The craniotomy was then filled with HEPES-buffered saline containing (in mM) 150 NaCl, 2.5 KCl, 10 HEPES, 2 CaCl_2 , 1 MgCl_2 (pH 7.4, adjusted with NaOH).

Single units were recorded from PCs in the right Crus II with a Multiclamp 700B or an Axopatch 200B amplifier (Molecular Devices, USA). Glass microelectrodes were filled with HEPES-buffered saline, and the resistance of the filled electrodes was 4–9 $\text{M}\Omega$. The pipette was advanced by 2- μm steps using a stepping micromanipulator (Narishige). PCs were recorded from relatively lateral areas of Crus II around 6+ (D1 zone) and 7+ (D2 zone) compartments. PCs were identified by the generation of simple and complex spikes. Electrophysiological data were recorded in the current clamp mode, low-pass filtered at 10 kHz, and digitized at 20 kHz, and acquired with Axograph X software (Axograph Scientific, Australia). Data were analyzed with Excel (Microsoft, USA) or OriginPro (OriginLab, USA). Data were high-pass filtered at 300 Hz to remove field potentials after recording. Peri-stimulus spike density functions (SDFs) were calculated by convolving the registered neuronal spikes with a Gaussian function (σ value = 3 ms).

For ION stimulation, the right side of the ION was exposed under a stereoscopic microscope (M60; Leica, Germany). The incision was made below the eye at 1 mm caudal to the mystacial pad. The muscles were dissected to expose the ION, and the cathode and anode of the bipolar tungsten electrodes (interpolar distance = 2 mm) were respectively placed on the afferent and efferent sides of the exposed ION. Stimuli (duration, 0.3 ms; amplitude, 1–4 mA) were applied every 3 s. The incidence of SSs showed a trend towards an increase with an increase in stimulus intensity, but became saturated (Figure S1). Stimulus strength was adjusted to evoke SSs at the highest incidence. For mechanical stimulation of the perioral area, air pressure

(0.34 MPa, 20 ms) was applied every 5 s using a PICOSPRTZER III (Parker, USA). The air-puff was delivered with a polyethylene tube (1 mm diameter) connected to a glass capillary (0.86 mm diameter) that was placed as close as possible to the right upper lip.

In some experiments, SDFs with clear 1st and 2nd SS peaks 0–34 ms after the ION stimulation were reassembled (Figures 1F, 2C, 2G, 2K, 2O, 4C, 5L, 5M, 5P, 5Q, 6D, and 6I). SS peaks were detected by first derivatives larger than mean + 1.5 s.d. of the baseline. Changes in the 1st and 2nd SS peaks (Figures 1G, 2D, 2H, 2L, 4D, 5L, 5M, 5P, 5Q, 6E, and 6J) were assessed by the absolute peak SDFs measured from the reassembled data (Figures 1F, 2C, 2G, 2K, 2O, 4C, 5L, 5M, 5P, 5Q, 6D and 6I). The Peak SDFs in muscimol and optogenetic experiments were measured as the largest SDF value within ± 2.0 ms of the 1st or 2nd SS peak before experimental manipulations. SS inhibition (Figures 1G, 2D, 2H, 2L, 4D, 6E, and 6J) were analyzed using all SDF data (Figures 1E, 2B, 2F, 2J, 2N, 4B, 6C and 6H). The averaged SDF during 40–200 ms after the ION stimulation was initially calculated, and then normalized to the baseline SDF before the ION stimulation (–500–0 ms) (normalized SS inhibition).

Changes in the 2nd SS peaks ($\Delta 2$ nd SS peak), represented by pseudocolor codes, caused by muscimol injections (Figures 1H, 3A, 4E, and 6K) or light administration (Figures 5K and 5O) were calculated using the following equation:

$$\Delta 2\text{nd SS peak} = \frac{2\text{nd SS peak}_{\text{after manipulation}} - 2\text{nd SS peak}_{\text{before manipulation}}}{2\text{nd SS peak}_{\text{before manipulation}}} \times 100(\%)$$

Changes in the normalized SS inhibition (Δ SS inhibition), represented by pseudocolor codes, induced by muscimol injections (Figures 1H, 3B, 4E, and 6L) were calculated using the following equation:

$$\Delta \text{SS inhibition} = \frac{\text{normalized SS inhibition}_{\text{after muscimol}} - \text{normalized SS inhibition}_{\text{before muscimol}}}{\text{normalized SS inhibition}_{\text{before muscimol}}} \times 100(\%)$$

At the end of the experiments, mice were deeply anaesthetized by overdose administration of the ketamine/xylazine mixture used for anesthetic induction and then fixed by transcardial perfusion with 4% paraformaldehyde (Nacalai Tesque or Wako, Japan) in 0.1 M phosphate buffer (PB) (pH 7.5). Fixed brains were processed for histological analysis.

Muscimol injections

A craniotomy (2–3 mm in diameter) was performed over the left cerebral cortex. Injections were performed from the dorso-rostral or dorso-lateral side into the target areas with the injection electrode tilted 20–45° from the horizontal plane. Muscimol (50 mM; Tocris, UK) and Chicago Sky Blue 6B (20 mg/ml; Sigma-Aldrich, USA) were dissolved in HEPES-buffered saline. A mixture of muscimol and Chicago Sky Blue 6B (70 nl per injection) was injected using a nano-injector equipped with a glass microelectrode (Nanoject II; Drummond, USA), with a flow rate of 23 nl/s.

After recording, mice were deeply anaesthetized by overdose administration of the ketamine/xylazine mixture, and then fixed by transcardial perfusion with 4% paraformaldehyde (Nacalai Tesque or Wako) in 0.1 M PB (pH 7.5). Coronal sections (100- μ m-thick) were cut with a microslicer, and then counterstained with cresyl violet solution (MUTO, Japan). Injection sites were confirmed by Chicago Sky Blue 6B staining and registered to the Allen Mouse Common Coordinate Framework (CCFv3)^{41,42–44} using Allen CCF tools⁷² in MATLAB (MathWorks, USA).

Virus injections

Mice were placed in a stereotaxic alignment system (RWD Life Science, USA) and maintained under ketamine (100 mg/kg)/xylazine (10 mg/kg) anesthesia. For expressing ArchT in cerebral neurons projecting to the MDJ or PG, AAVrg-CamKII-*ArchT*-GFP (titer $\geq 7 \times 10^{12}$ vg/ml; plasmid #99039, Addgene, USA), which permits retrograde-expression of *ArchT*-GFP in projection neurons, was infused (0.1–0.2 μ l) into the MDJ and PG (0.1–0.12 μ l) with Hamilton syringes (Hamilton, USA). Then, 5 weeks later, optogenetic experiments were performed. After the experiments, mice were transcardially fixed by perfusion of 4% paraformaldehyde dissolved in 0.1 M PB. Fixed brains were processed for histological analysis.

Optogenetics

Five weeks after virus vector injections, mice were anaesthetized with a mixture of ketamine (100 mg/kg) and xylazine (10 mg/kg). A craniotomy over the left MII to SII was performed, and the dura was removed. A 2 × 5 square grid (pitch = 1 mm, bar width = 0.05 mm) was placed on the cortical surface, as shown in Figure 5I. First, 50 control SS recordings following right ION stimulation without light were performed. Thereafter, a plastic optical fiber (0.4 mm diameter) was placed in one of the grid columns on the brain using a micromanipulator (Narishige). Yellow light (575 nm) was generated using laser diodes (SPECTRA X; Lumencor, USA) and applied through the optical fiber for 180 ms starting at 100 ms before the onset of each ION stimulation (50 times) with an intensity of 17.6 mW (160 mW/mm²) measured at the tip of the optical fiber. After recording from a grid column, the optical fiber was systematically moved to other columns.

GABA_AR blocker perfusion

After the cerebellar craniotomy, the craniotomized region of bone was surrounded by embankments made of acrylic resin equipped with two polyethylene tubes for perfusion of the external solution. To block inhibitory synaptic transmission in the cerebellar cortex, the surface of the cerebellar cortical recording area was perfused with 20 μM SR95531 (Tocris), a GABA_A receptor antagonist, at a constant speed of 1 ml/min at 36 ± 2°C.

Retrograde tracer injections

Under ketamine (100 mg/kg)/xylazine (10 mg/kg) anesthesia, a glass pipette filled with fluorogold (FG; Wako, Japan) dissolved in saline was inserted stereotaxically into the left PG, MDJ and PRNc. FG (15 nl) was pressure-injected using a nanoinjector (Nanoject II), at a flow rate of 23 nl/s. After 4 days of recovery, mice were deeply anaesthetized with the ketamine/xylazine mixture, and transcardially fixed by perfusion of 4% paraformaldehyde dissolved in 0.1 M PB. Fixed brains were processed for histological analysis.

Histological analysis

Fixed brains were post-fixed with paraformaldehyde solution and then immersed in 25% sucrose in 0.1 M PBS (pH 7.4). Post-fixed brains were embedded in optimal cutting temperature compound (Sakura Finetek, Japan) and frozen. Coronal sections (50-μm-thick) were cut with a cryostat (Leica). Slices were counterstained with NeuroTrace 500/525 Green Fluorescent Nissl Stain (Thermo Fisher Scientific, USA) for FG injected brains, and with NeuroTrace 530/615 Red Fluorescent Nissl Stain for AAV-injected brains. Images were taken with a fluorescence microscope (BZ-9000; Keyence, Japan).

Hierarchical clustering analysis

Data were standardized, and then hierarchical clustering was performed with 'Euclidean' as the metric and 'ward' linkage to calculate cluster distances with the ClusterMap tool in the Python package, Seaborn. The package internally uses the scientific Python module cluster (scipy.cluster) for clustering and the matplotlib package for visualization.

QUANTIFICATION AND STATISTICAL ANALYSIS

For all experiments, mice were randomly allocated to experimental groups, with *n* representing the number of PCs. Data in the figures are presented as the mean ± SEM. Statistical significance was assessed by paired *t*-test or the Wilcoxon signed-rank test, depending on whether the data sets passed the normality test and equal variance test, unless otherwise stated in the text. Statistical comparisons among three or more groups were conducted using one-way ANOVA. When differences were judged to be significant, data were processed using the Holm-Šidák *post-hoc* test. Differences between groups were considered significant at **p* < 0.05. Data handling and statistical analyses were performed with Excel (Microsoft), SigmaPlot 12.5 (RRID: SCR_010285, Systat Software, USA) or OriginPro (OriginLab).